



PCCP

In-Situ Observation of Potential-Dependent Structure of Electrolyte/Electrode Interface by Heterodyne-Detected Vibrational Sum Frequency Generation

Journal:	<i>Physical Chemistry Chemical Physics</i>
Manuscript ID	CP-ART-11-2019-006253.R1
Article Type:	Paper
Date Submitted by the Author:	20-Dec-2019
Complete List of Authors:	Sayama, Atsushi; Tokyo Institute of Technology, Chemistry; RIKEN, Molecular Spectroscopy Laboratory Nihonyanagi, Satoshi; Rikagaku Kenkyujo, Molecular Spectroscopy Laboratory Ohshima, Yasuhiro; Tokyo Institute of Technology, Department of Chemistry Tahara, Tahei; RIKEN, Molecular Spectroscopy Lab

SCHOLARONE™
Manuscripts

ARTICLE

In-Situ Observation of Potential-Dependent Structure of Electrolyte/Electrode Interface by Heterodyne-Detected Vibrational Sum Frequency Generation

Received 00th January 20xx,
Accepted 00th January 20xx

DOI: 10.1039/x0xx00000x

Atsushi Sayama,^{a,b} Satoshi Nihonyanagi,^{*a,c} Yasuhiro Ohshima^b and Tahei Tahara^{*a,b,c}

Elucidating the structure of electrolyte/electrode interfaces is of essential importance not only for understanding of the fundamental process of electrochemistry but also for developing next-generation rechargeable batteries. In this study, we applied HD-VSFG spectroscopy to study a prototypical non-aqueous electrochemical interface of a platinum electrode in 0.1 M LiCF₃SO₃ acetonitrile (CH₃CN) solution, and measured Imχ⁽²⁾ spectra by changing the applied potential in the range of -0.8 V to 2.0 V. In the positive potential region, the positive bands assignable to acetonitrile appear in the CH₃ and CN stretch regions, and their positive signs indicate the CH₃-down orientation of acetonitrile at the interface. We also observed SO₃⁻ stretch band of the anion of electrolyte and found that the potential dependence of its intensity is similar to those of the CH₃ and CN bands of acetonitrile. These observations indicate that the CF₃SO₃⁻ anion is adsorbed at the platinum surface in the positive potentials, which induces CH₃-down orientation of acetonitrile at the interface. The present study demonstrates the advantage of HD-VSFG spectroscopy for studying electrochemical systems, and it opens a new way to investigate the electrolyte/electrode interfaces at the molecular level.

1. Introduction

Molecular-level elucidation of structure and electrochemical reactions at electrolyte/electrode interfaces is of essential importance not only for understanding of the fundamental processes in electrochemistry but also for industrial applications such as development of next-generation rechargeable batteries¹⁻³. For achieving this goal, huge efforts have been made using various techniques such as X-ray scattering⁴⁻⁶, IR⁷⁻¹⁰, and Raman¹¹⁻¹⁴ spectroscopy. Despite its importance and efforts, however, the structure and electrochemical reactions at the electrolyte/electrode interfaces have not been well understood at the molecular level because of the complexity of the electrochemical interfaces. Therefore, further development of advanced in-situ characterization methods is necessary for obtaining molecular-level knowledge about the electrolyte/electrode interfaces.

Vibrational sum frequency generation (VSFG) is one of the second-order nonlinear optical processes which are intrinsically interface-selective.¹⁵⁻¹⁷ In the VSFG process, two laser pulses having

visible (ω_{vis}) and infrared (ω_{IR}) frequencies are irradiated onto a sample, and sum frequency (SF) light $\omega_{\text{SF}} = \omega_{\text{vis}} + \omega_{\text{IR}}$ is generated in a region where inversion symmetry is broken. While most of bulk phases have inversion symmetry, the interface regions do not. Therefore, VSFG can selectively detect the response of the interfacial molecules. Furthermore, when ω_{IR} matches with a vibrational transition of the interfacial molecules, the SF signal is resonantly enhanced. Thus, VSFG can provide vibrational spectra of only molecules at the interface, and hence it has been widely utilized for studying various interfaces.^{16, 18-21}

In spite of its unique interface selectivity, conventional VSFG spectroscopy has a crucial problem: Because conventional VSFG detects the intensity of the SF signal with homodyne detection, it can only provide the spectra that correspond to the absolute square of the second-order nonlinear susceptibility, $|\chi^{(2)}|^2$. In such $|\chi^{(2)}|^2$ spectra, the interference between resonant and non-resonant signals and/or that between different vibrational resonances distort spectral features, and the sign of $\chi^{(2)}$ is lost. These drawbacks of conventional VSFG spectroscopy has generated numbers of controversies about the interpretation of the VSFG spectra.^{22, 23}

In the last decade, an advanced VSFG spectroscopy, i.e., heterodyne-detected VSFG (HD-VSFG), has been developed. This new method has been applied to various interfaces such as air/water, air/ice and silica/water interfaces, and provided new insights into the structure and dynamics at the interfaces.²⁴⁻³¹ In HD-VSFG spectroscopy, $\chi^{(2)}$ itself is directly determined by analyzing the interference between the SF signal and local oscillator (LO). Therefore, the experimentally obtained spectra are free from the spectral distortion and hence can be interpreted straightforwardly in the same way as we interpret IR absorption and/or Raman spectra. Moreover, the up/down

^a Molecular Spectroscopy Laboratory, RIKEN, Wako, Saitama 351-0198, Japan.

^b Department of Chemistry, Tokyo Institute of Technology, Meguro, Tokyo 152-8551, Japan.

^c Ultrafast Spectroscopy Team, RIKEN Center for Advanced Photonics (RAP), Wako, Saitama 351-0198, Japan.

† Footnotes relating to the title and/or authors should appear here.

Electronic Supplementary Information (ESI) available: 1. Estimation of thickness of the solution layer, 2. Contribution of the $\chi^{(3)}$ effect, 3. Contribution of the CaF₂/acetonitrile solution interface, 4. $\chi^{(2)}$ spectra of the air/acetonitrile interface, 5. Estimation of the IR loss due to the absorption by the CF₃SO₃⁻ anion in the solution layer in the SO₃⁻ stretch region, 6. Bulk IR and Raman spectra of 0.1 M LiCF₃SO₃ in acetonitrile solution, 7. Fitting analysis. See DOI: 10.1039/x0xx00000x

ARTICLE

orientation of interfacial molecules is experimentally determined from the sign of the imaginary part of $\chi^{(2)}$. This is a unique advantage of HD-VSFG spectroscopy over any other interface spectroscopies.

Electrochemical interfaces are the core of electrochemistry, and they have been one of the most important subjects of VSFG spectroscopy for many years.³²⁻⁴² However, most of previous electrochemical VSFG studies were carried out by conventional VSFG with homodyne detection because it is difficult to determine the phase and amplitude of the SF signal at buried interfaces, particularly under an electrochemical environment. In other words, it is difficult to measure a reference spectrum for calibration under the same condition as the sample measurement because of the presence of the electrolyte solution and the optical window. Actually, Zanni and coworkers applied HD-VSFG spectroscopy to a CO-adsorbed electrode interface,⁴³ but they did not discuss the sign of $\chi^{(2)}$ at the electrolyte/electrode interface because of the lack of the phase reference. To overcome this problem, we developed the in-situ reference method very recently, which has enabled us to determine the phase and amplitude the $\chi^{(2)}$ spectrum at electrolyte/electrode interfaces.⁴⁴

In the present study, by using this in-situ reference method, we apply HD-VSFG spectroscopy to a prototypical non-aqueous electrochemical interface, i.e., the interface between a platinum electrode and 0.1 M LiCF₃SO₃ acetonitrile (CH₃CN) solution. Surprisingly, our HD-VSFG experiments clearly indicate that the CH₃ group of acetonitrile points toward the platinum electrode at positive electrode potentials, which is counter-intuitive and is opposite to the orientation proposed by a previous conventional VSFG study.³³ Supported by additional data obtained with conventional VSFG experiments, we conclude that this orientation of acetonitrile molecules is induced by the anion adsorbed on the electrode surface at the positive potentials. This is the first experimental observation of the potential-dependent up/down orientation of molecules at the electrolyte/electrode interface, which is essential for obtaining the molecular-level picture of the electrochemical interfaces.

2. Experimental

The optical setup of HD-VSFG measurement (Fig. 1a) has been described in detail elsewhere.^{24, 25} Briefly, near-infrared laser pulse (center wavelength: 796 nm) is generated by Ti:Sapphire regenerative amplifier (Solstice, Spectra Physics, pulse energy: ~3 mJ, repetition rate: 1 kHz, pulse width: 100 fs). The 2/3 of the 796-nm output pulse was introduced into an optical parametric amplifier equipped with a difference frequency generation unit (TOPAS-prime, Spectra Physics) for generating tunable broad band IR pulses (1000 - 4000 cm⁻¹) which were used as ω_R . The other 1/3 of the output was narrowed (~5 cm⁻¹) by a 4f grating filter consisting of a holographic grating (1800 g/mm), mechanical slit and cylindrical lens ($f = 300$ mm), and

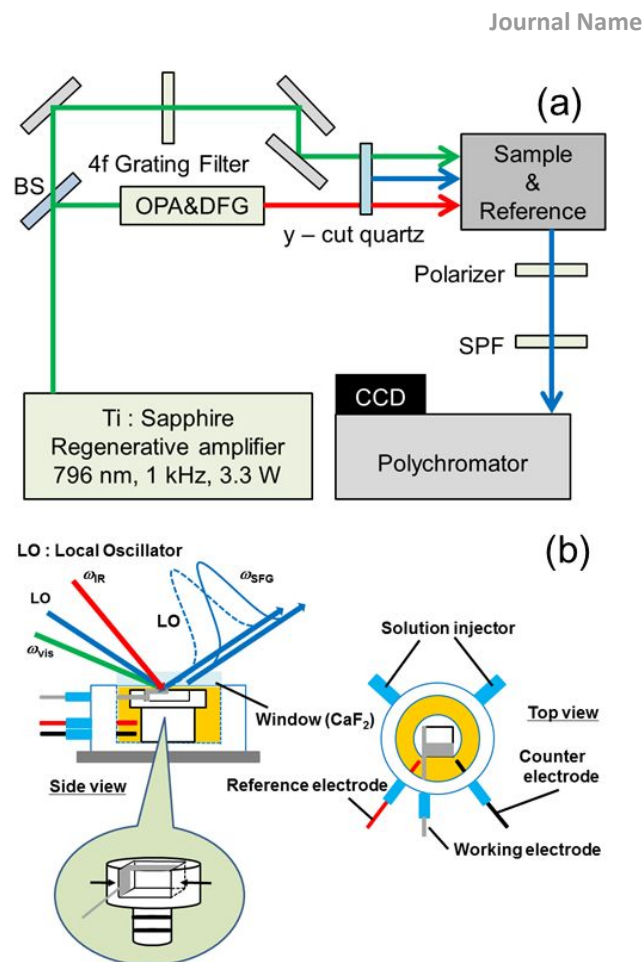


Fig. 1 Schematic of the experimental setup. (a) The optical setup. BS: Beam Splitter, SPF: Short Pass Filter. (b) Spectro-electrochemical cell developed for HD-VSFG measurements.

was used as ω_{vis} . The ω_{vis} and ω_R pulses were focused onto a thin plate of y-cut quartz (10 μ m thick), which generates a local oscillator, ω_{LO} . The ω_{LO} passes through a 3 mm thick silica plate which delays the ω_{LO} by T (~5 ps) compared to ω_{vis} and ω_R . The ω_{vis} , ω_R and delayed ω_{LO} pulses were focused onto the electrolyte/electrode interface with incident angle of ca. 30°, 27° and 29°, respectively. The generated SF light from the electrode and the reflected ω_{LO} were introduced to a polychromator (Andor Tech., SR3031-A) and detected by a CCD (Andor Tech., Newton DU970P). All measurements were performed with PPP combination (P-polarized ω_{SFG} , P-polarized ω_{vis} , P-polarized ω_R).

In order to obtain a reference spectrum relevant to the electrolyte/electrode interface, we used a metal electrode hybridized with the reference material: a thin film platinum electrode deposited on a half of z-cut quartz substrate (10×10×3 mm).⁴⁴ In this case, the sample electrode and reference quartz are located underneath a common optical window and electrolyte solution, and the sample and reference spectra can be measured simply by horizontally moving the cell using a motored stage. This makes it possible to keep the optical path lengths of the input pulses and SF light the same for the sample and reference measurements, allowing reliable calibration for the phase and amplitude. (The thickness of the metal electrode

is ca. 100 nm so that the corresponding difference in the optical path length due to the thickness of the metal electrode does not practically affect the phase calibration.⁴⁴) The loss of the input IR light due to the absorption by the solution phase is also the same in the sample and reference measurements and hence it is canceled out with the amplitude normalization. Thus, the proper $\text{Im}\chi^{(2)}$ spectra of the electrolyte/electrode interface are obtainable by normalizing the complex fringe spectrum of the acetonitrile/platinum interface by that of the acetonitrile/quartz reference interface.

The HD-VSFG measurement was performed with a home-made spectro-electrochemical cell whose body is made of polypropylene (Figure 1b). In this cell, the sample substrate was pushed against a CaF_2 optical window to make the electrolyte solution layer very thin. The typical thickness of the electrolyte solution layer between the CaF_2 window and the sample substrate was estimated to be $\sim 8 \mu\text{m}$ (See SI). About half of the top surface of the z-cut quartz substrate was covered by polycrystalline platinum which was deposited by an electron beam evaporator. This part was used as the working electrode. A platinum wire and a silver wire (Ag/Ag^+) were used as the counter electrode and the reference electrode, respectively. The potential of Ag/Ag^+ was calibrated by the redox potential of ferrocene/ferrocene⁺. The potential of the Ag/Ag^+ reference electrode was around +0.26 V with respect to the saturated calomel electrode (SCE). In this study, the electrode potential was quoted against the Ag/Ag^+ reference. The cyclic voltammetry was performed with a function generator (NF Corporation, WF1943A) and a potentiostat (HOKUTO DENKO, HA-151).

The sample substrate was immersed in concentrated sulfuric acid overnight and rinsed with copious amount of water. Then it was gently annealed near gas/ O_2 flame before in-situ electrochemical HD-VSFG measurements. After the flame annealing, the sample substrate was put into acetonitrile solution immediately to prevent surface contamination. The acetonitrile (Sigma-Aldrich, anhydrous grade) was used as a solvent and LiCF_3SO_3 (Kishida Chemical Co., lithium battery grade) was used as an electrolyte without further purification. All reagents were kept in a glove box filled in Ar gas till the HD-VSFG experiments.

All the vibrational bands in the VSFG spectra obtained in the present study are attributable to the molecules at the very vicinity of the electrode interface, and the contribution from other sample regions such as the oriented molecules in the diffuse electric double layer (so called $\chi^{(3)}$ effect)²⁷ and the CaF_2 /electrolyte interface are considered negligible (See SI for detailed discussions).

3. Results and Discussion

3-1. Cyclic voltammetry

Two cycles of cyclic voltammetry were carried out between -0.8 V and 2.0 V at a scan rate of 10 mV/s prior to the spectroscopic measurements. Figure 2 shows the cyclic voltammogram of 0.1 M LiCF_3SO_3 acetonitrile solution. The current density (i.e., the vertical

axis) in this figure was calculated using the surface area of the platinum electrode which was obtained from the flowed charge of hydrogen desorption in sulfuric acid aqueous solution. The very low current density indicates that no electrochemical reaction happens in this potential region, and only an electric double layer is charged. The slight tilt of the voltammogram suggests that the resistance of the thin-solution layer is high in the present electrochemical cell. To minimize the effect of this high resistance, we waited for 6 minutes after changing the electrode potential before the spectroscopic measurement to allow the system to reach the equilibrium.

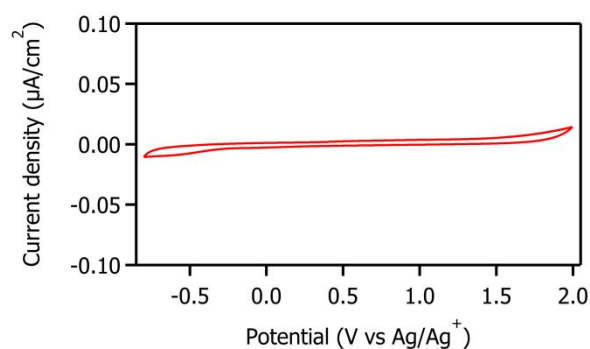


Fig.2 The cyclic voltammogram of 0.1 M LiCF_3SO_3 acetonitrile solution. The scan rate was 10 mV/s.

3-2. HD-VSFG spectra in the CH stretch region

Figure 3 shows the CH stretch region of the $\chi^{(2)}$ spectra of the acetonitrile/platinum interface with 0.1 M LiCF_3SO_3 electrolyte, which were measured with changing the electrode potential between -0.8 V and 2.0 V with a 0.4 V potential increment. At 0.4 V which is close to the open circuit potential, the $\text{Im}\chi^{(2)}$ spectrum shows a small positive (upward) band at 2940 cm^{-1} . The amplitude of this band increases as the electrode potential becomes more positive. On the other hand, it decreases as the electrode potential becomes more negative and finally disappears almost completely at -0.8 V. The peak frequency of this band is close to the absorption maxima of the neat acetonitrile in the bulk (2944 cm^{-1}).⁴⁵ Because it is known that the CH stretch band exhibits a red-shift when it strongly interacts with the electrode surface,⁴⁶ the positive band at 2940 cm^{-1} is assignable to the CH_3 symmetric stretch mode of the acetonitrile molecules that are not directly bound to the electrode.

For free acetonitrile, the hyperpolarizability of the CH_3 symmetric stretch is known to be negative.⁴⁷ Therefore, the positive CH_3 symmetric band in the $\text{Im}\chi^{(2)}$ spectra indicates CH_3 -down orientation, i.e., the CH_3 group of acetonitrile is pointing toward the platinum electrode. This result differs from the argument of a previous homodyne VSFG study by Baldelli and co-workers.³³ In their work, the orientation of acetonitrile was assumed to be CH_3 -up, considering the electrostatic interaction between the lone pair electron on nitrogen and the positively charged electrode.³³ However, the heterodyne detection realized in the present study experimentally determined the sign of the $\text{Im}\chi^{(2)}$ signal and revealed that this is not the case. In

order to confirm our conclusion, we also measured the $\text{Im}\chi^{(2)}$ spectrum of acetonitrile at the air/neat acetonitrile interface (Figure S3). At the air/neat acetonitrile interface, acetonitrile is expected to have CH_3 -up orientation because the CH_3 group is more hydrophobic compared to the CN group. The sign of the CH_3 band in the $\text{Im}\chi^{(2)}$ spectrum is indeed negative (Figure S3), which confirms that the negative CH_3 band corresponds to the CH_3 -up orientation at the air/neat acetonitrile interface. Therefore, the positive CH_3 band observed at the acetonitrile/platinum interface surely shows that acetonitrile at the interface takes CH_3 -down orientation. We will discuss later why acetonitrile prefers the counter-intuitive CH_3 -down orientation at the electrode interface. If the up/down orientation of acetonitrile changes with the electrode potential, the sign change of the CH_3 band is expected. However, no clear negative band is observed in the potential range examined in the present study.

Figure 3 also shows the $|\chi^{(2)}|^2$ spectra (blue broken lines) which were calculated from the $\chi^{(2)}$ spectra obtained with HD-

around 2950 cm^{-1} , and the peak intensity increases as the potential becomes more positive. On the other hand, at the potentials ranging from 0.8 V to -0.4 V , a small dip appears at around 2930 cm^{-1} . These features of the $|\chi^{(2)}|^2$ spectra are qualitatively consistent with the spectra reported in a previous homodyne VSFG study.³³ In the previous study, the strong peak observed at 2940 cm^{-1} in the positive potential region was assigned to the CH_3 symmetric stretch of acetonitrile which is pointing away from the electrode (CH_3 -up) whereas the red-shifted dip feature was assigned to the CH_3 symmetric stretch of acetonitrile that directly interacts with the electrode with CH_3 -down orientation.³³ However, the $\text{Im}\chi^{(2)}$ spectra obtained in this study show no negative peak at 2930 cm^{-1} , and therefore it is now clear that the dip feature in the $|\chi^{(2)}|^2$ spectra is indeed an artifact that appears when the $\text{Re}\chi^{(2)}$ approaches closely to zero. This demonstrates that HD-VSFG spectroscopy is critically important also for the study of electrochemical interfaces.

It is noteworthy that the vibrationally non-resonant background, $\chi^{(2)}_{\text{NR}}$, appears both in the $\text{Im}\chi^{(2)}$ and $\text{Re}\chi^{(2)}$ spectra,

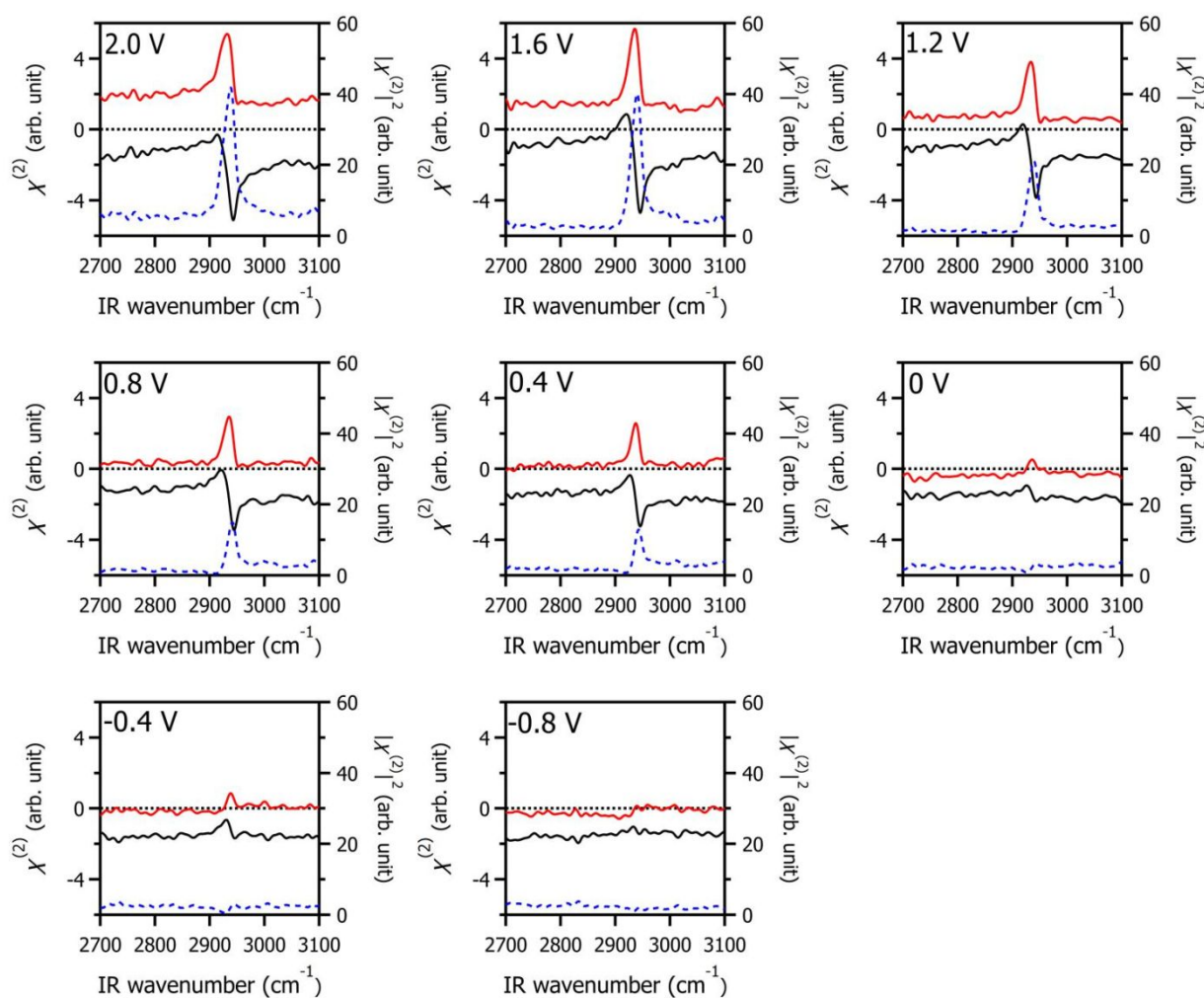


Fig. 3 The $\text{Im}\chi^{(2)}$, $\text{Re}\chi^{(2)}$ and $|\chi^{(2)}|^2$ spectra of the acetonitrile/platinum interface with $0.1\text{ M LiCF}_3\text{SO}_3$ electrolyte in the CH stretch region. The red curve, black curve and blue broken curve are $\text{Im}\chi^{(2)}$, $\text{Re}\chi^{(2)}$ and $|\chi^{(2)}|^2$, respectively. The electrode potential with respect to Ag/Ag^+ is shown on top of each spectrum. The $|\chi^{(2)}|^2$ spectra were calculated from the $\text{Im}\chi^{(2)}$ and $\text{Re}\chi^{(2)}$ spectra.

VSFG measurements. These $|\chi^{(2)}|^2$ spectra show a peak at 2950 cm^{-1} and $\chi^{(2)}_{\text{NR}}$ in the $\text{Im}\chi^{(2)}$ spectra substantially changes with the

change of the electrode potential. In Figure 4a, the amplitude of $\chi^{(2)}_{\text{NR}}$ is plotted as a function of the potential. It is clear that $\chi^{(2)}_{\text{NR}}$ in the $\text{Im}\chi^{(2)}$ spectrum does not show a noticeable change in the negative potential region but it goes to positive in the positive potential region. On the other hand, $\chi^{(2)}_{\text{NR}}$ in the $\text{Re}\chi^{(2)}$ spectrum does not significantly vary with the potential. Although the value of $\chi^{(2)}_{\text{NR}}$ differs depending on the sample, this trend of the potential dependence of $\chi^{(2)}_{\text{NR}}$ is well reproducible.

The origin of the $\chi^{(2)}_{\text{NR}}$ in the $\text{Im}\chi^{(2)}$ spectra at the electrode interface is not clear at the moment. However, in general, $\chi^{(2)}_{\text{NR}}$ in the $\text{Im}\chi^{(2)}$ spectrum is attributed to either electronic resonance⁴⁸ or bulk contribution.^{49, 50} Although the latter has been considered the origin of $\chi^{(2)}_{\text{NR}}$ in the $\text{Im}\chi^{(2)}$ spectrum at dielectric interfaces,^{49, 50} it is not likely the case for the metal electrode because the charge of the metal electrode is localized only at the metal surface and hence it is difficult to imagine that the property of bulk metal changes with the potential. As for the former, it is known that platinum has no inter-band transition in the visible range.⁵¹ Therefore, we consider that the $\chi^{(2)}_{\text{NR}}$ in the $\text{Im}\chi^{(2)}$ spectra is likely attributable to the intra-band transition induced by the IR photon. The density of states of the neutral platinum is known to be very large below the Fermi level while it is small above it.⁵² Therefore, it is possible that when the positive potential is applied, i.e., the Fermi level is lowered, abundant unoccupied states become available to absorb IR photons, which increases $\chi^{(2)}_{\text{NR}}$ in $\text{Im}\chi^{(2)}$. On the other hand, even if the negative potential is applied, i.e., the Fermi level gets higher, the density of unoccupied states does not increase and hence it does not increase the intra-band transition. This expected behavior is consistent with the observed asymmetric potential dependence.

An important observation is that the phase of $\chi^{(2)}_{\text{NR}}$ of the platinum electrode changes with the potential. Indeed, the phase of $\chi^{(2)}_{\text{NR}}$ changes by as large as 60°, as clearly seen in Fig 4b. To our knowledge, this is the first explicit observation of the phase shift of $\chi^{(2)}_{\text{NR}}$ at the electrode interface during the potential scan. Such a potential-dependent phase shift of $\chi^{(2)}_{\text{NR}}$ makes the fitting analysis of homodyne VSG spectra even more difficult, and therefore the direct measurement of complex $\chi^{(2)}$ with HD-VSG is important also in this regard.

3-3. HD-VSG spectra in the CN stretch region

Figure 5 shows $\chi^{(2)}$ and $|\chi^{(2)}|^2$ spectra in the CN stretch region of the acetonitrile/platinum interface with 0.1 M LiCF_3SO_3 electrolyte. Because strong IR absorption of atmospheric CO_2 disturbs the spectra in the frequency region of 2300 – 2400 cm^{-1} , we only show the spectra in the 2000 – 2300 cm^{-1} region. At the positive potentials, the $\text{Im}\chi^{(2)}$ spectra exhibit two positive bands at 2245 and 2290 cm^{-1} , which are assignable to the CN stretch vibration of free acetonitrile and its Fermi resonance with a combination band, respectively.^{33, 45} The amplitudes of these positive bands decrease as the electrode potential becomes more negative. The corresponding change can also be seen in the $|\chi^{(2)}|^2$ spectra. In fact, this change of the $|\chi^{(2)}|^2$ spectra has been reported in the previous homodyne VSG study.³³ At the air/acetonitrile interface, the CN stretch band of acetonitrile appears with the negative sign (Fig. S3). Because the acetonitrile molecule is expected to have the CN-down

orientation at the air/acetonitrile interface, the opposite positive sign of the CN stretch band at the acetonitrile/platinum interface indicates the CN-up orientation of acetonitrile molecules. This conclusion is consistent with the $\text{Im}\chi^{(2)}$ spectra in the CH_3 stretch region which indicates the CH_3 -down orientation. In addition to the sharp vibrational resonance features due to the CN stretch (split by the Fermi resonance), a positive offset-like signal is observed in the $\text{Im}\chi^{(2)}$ spectra at the positive potentials, which is again consistent with the observation in the CH_3 stretch region. Consequently, the $\text{Im}\chi^{(2)}$ spectra in the CN region at the positive potentials accord well with those in the CH_3 stretch region (Fig. 3) which were discussed in the previous section.

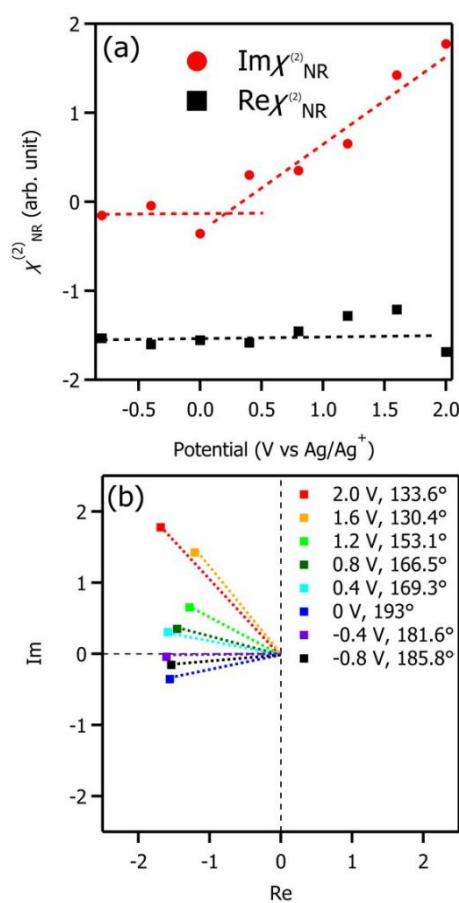


Fig. 4 Electrode potential dependence of $\chi^{(2)}_{\text{NR}}$. (a) Amplitude of $\chi^{(2)}_{\text{NR}}$. The broken lines are eye-guide. (b) Phase of $\chi^{(2)}_{\text{NR}}$. The phase angle at each potential is written in the legend.

In the potential region more negative than 0.8 V, a very broad negative band appears around 2150 cm^{-1} . Such a broad band in the low frequency region has been observed in several different spectroscopic measurements, including subtractively normalized interfacial IR spectroscopy⁵³ and surface enhanced Raman spectroscopy¹⁴. Initially, this band was assigned to the CN stretch of acetonitrile that is directly attached on the platinum surface,^{53, 54} but later many groups re-assigned this band to the stretch vibration of the adsorbed CN^- which is produced by the catalytic decomposition at the platinum

surface^{14, 55, 56}. In homodyne VSFG studies, the broad 2150 cm⁻¹ band has also been observed when the system contains CN⁻ ions in solution⁵⁵ or a hot platinum electrode was immersed in an acetonitrile solution⁵⁶. Therefore, we assign this band to the adsorbed CN⁻. We note that no CH band is observed in the negative potential region where this 2150 cm⁻¹ band is observed (e.g. -0.8 V). This implies that the relevant chemical species has the CN moiety but not the CH group, being consistent with this assignment.

It is noteworthy that the 2150-cm⁻¹ band was not observed in the previous SFG study of acetonitrile/platinum interface by Baldelli et al.³³ Gu et al. proposed that CN⁻ is produced at a roughened platinum electrode at negative potentials but not at a smooth Pt(111) surface.^{14, 57} Because Baldelli et al. used a single crystal whereas we used evaporated thin film in this study, the lack of the 2150 cm⁻¹ band in the spectra reported by Baldelli et al. is highly likely attributable to the difference in the roughness of the platinum electrode used in the two experiments.

Intuitively, it is considered that acetonitrile prefers the CH₃-up & CN-down orientation at the acetonitrile/platinum electrode at positive potentials owing to attractive electrostatic interaction between the lone pair electron on nitrogen and the positively charged electrode.³³ However, the present HD-VSFG experiments clearly indicate that acetonitrile has the opposite orientation at the interface at the positive potentials, i.e., the CH₃-down and CN-up orientation at the positive potentials. In order to rationalize this counter-intuitive orientation of acetonitrile at the positive potentials, we consider the possibility that the anion is adsorbed on the electrode and that this anion interacts with acetonitrile at the vicinity of the interface. In other words, we hypothesize that CH₃-down and CN-up orientation of acetonitrile is induced by the repulsive interaction between the lone pair electron on nitrogen and negative charge of anions.

To verify the above-mentioned hypothesis, we measured Im $\chi^{(2)}$ spectra of a pure acetonitrile/platinum interface without the electrolyte to examine the influence of anion to the orientation of acetonitrile. Fig. 6a shows the Im $\chi^{(2)}$ spectrum in the CN stretch region at the pure acetonitrile/platinum interface in the open circuit

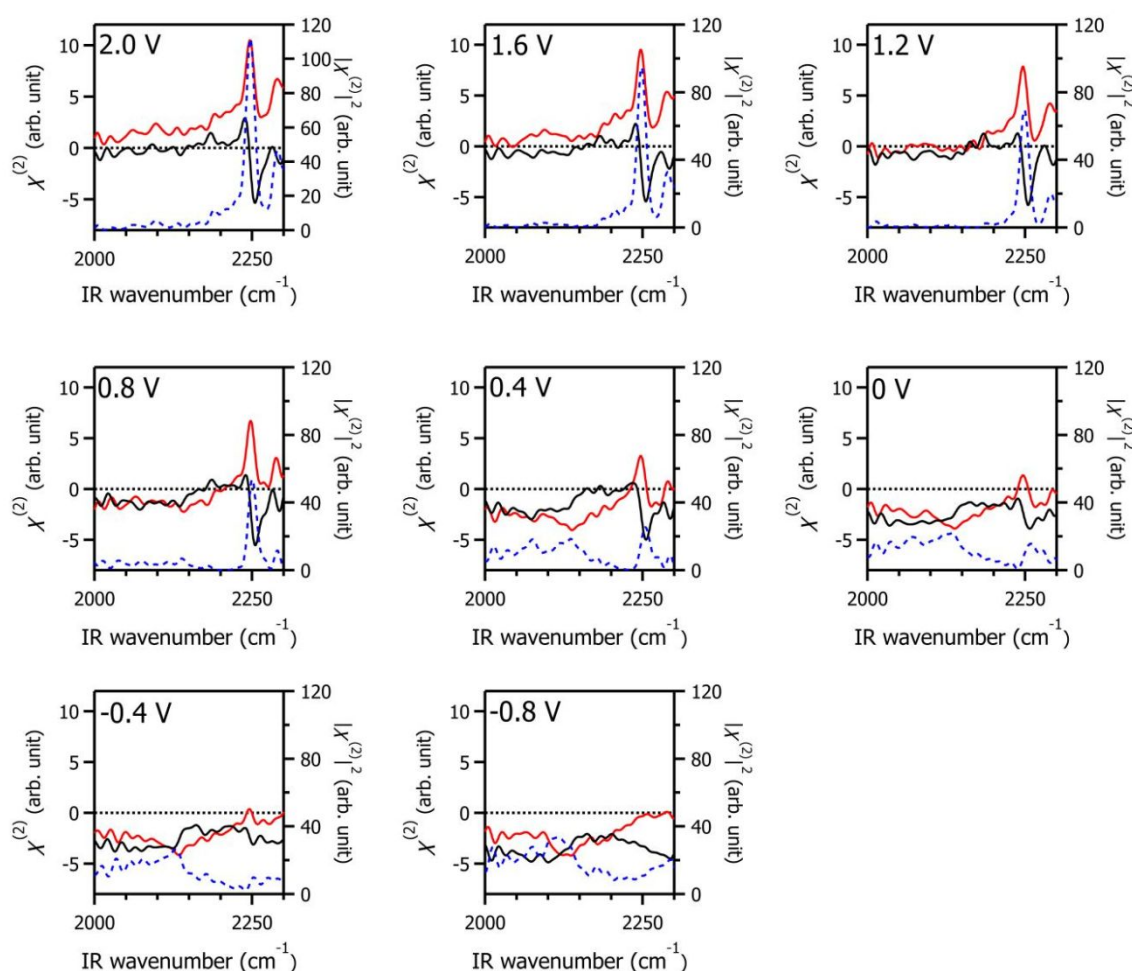


Fig. 5 The Im $\chi^{(2)}$, Re $\chi^{(2)}$ and $|\chi^{(2)}|^2$ spectra of acetonitrile/platinum interface with 0.1 M LiCF₃SO₃ electrolyte in the CN stretch region. Red curve, black curve and blue broken curve are Im $\chi^{(2)}$, Re $\chi^{(2)}$ and $|\chi^{(2)}|^2$, respectively. The electrode potential with respect to Ag/Ag⁺ is shown on top of each spectrum. The $|\chi^{(2)}|^2$ spectra were calculated from the Im $\chi^{(2)}$ and Re $\chi^{(2)}$ spectra.

3-4. HD-VSFG spectra without electrolyte

condition. While a broad negative band (due to the adsorbed CN⁻) is observed at 2200 cm⁻¹, any positive band assignable to the acetonitrile is hardly observed at 2245 cm⁻¹. This observation is

consistent with the $\text{Im}\chi^{(2)}$ spectrum in the CH stretch region shown in Fig. 6b, which does not exhibit any clear peak at 2940 cm^{-1} due to the CH_3 stretch of acetonitrile. These results indicate that free acetonitrile at the pure acetonitrile/platinum interface without ions is not preferentially oriented either CH_3 -up or CH_3 -down, suggesting an essential role of the anion to induce CH_3 -down orientation of acetonitrile observed with the electrolyte.

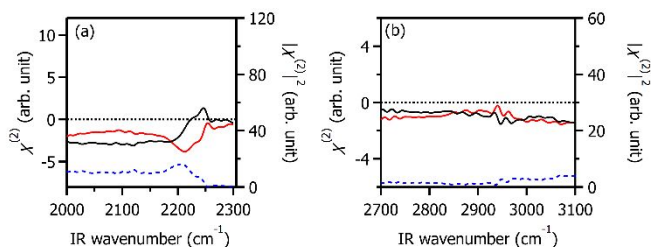


Fig. 6 The $\chi^{(2)}$ spectrum of pure acetonitrile/platinum interface in (a) the CN stretch region and (b) the CH stretch region. Red solid, black solid, and blue broken curves correspond to $\text{Im}\chi^{(2)}$, $\text{Re}\chi^{(2)}$, and $|\chi^{(2)}|^2$, respectively. The $|\chi^{(2)}|^2$ spectra were calculated from the $\text{Im}\chi^{(2)}$ and $\text{Re}\chi^{(2)}$ spectra. The electrode potential is not under control without the electrolyte.

3-5. VSFG spectra of CF_3SO_3^- anion

In order to directly prove the existence of the anion on the electrode and clarify its potential-dependent adsorption, we measured VSFG spectra in the $950 - 1200\text{ cm}^{-1}$ region where the vibration of CF_3SO_3^- anion appears. We performed experiments with conventional homodyne VSFG measurements, not by HD-VSFG, because quartz cannot be used as the reference in this low frequency region due to the vibrational resonances of quartz itself. Nevertheless, the VSFG spectra obtained with homodyne detection are normalized by an air/gold spectrum to correct the effect of the intensity distribution of the ω_{IR} spectra. Although this normalization does not take account of the absorption of the CF_3SO_3^- anion, the effect is not large in the present experiment, as described in SI (Figure S4).

Fig. 7 shows the obtained $|\chi^{(2)}|^2$ spectra at the acetonitrile/platinum interface with $0.1\text{ M LiCF}_3\text{SO}_3$ electrolyte. Black broken curves are the fitted curves obtained with the square of Lorentz function described in SI. At the potentials more positive than 0.4 V , a clear band is observed at 1040 cm^{-1} , and its intensity increases as the electrode potential becomes more positive. Based on the frequency, this band is assignable to the SO_3^- symmetric stretch mode of the CF_3SO_3^- anion.⁵⁸⁻⁶⁰ The appearance of this 1040 cm^{-1} band directly proves the adsorption of the CF_3SO_3^- anion on the electrode at positive potentials. The spectra also indicate that the anion desorbs from the electrode at the negative potentials. Qualitatively, the potential dependence of the intensity of the SO_3^- symmetric band appears similar to that of the CH_3 symmetric and CN stretch bands of acetonitrile (Figs. 3 and 5). We note that CF_3SO_3^- anion is expected to also show the CF_3 anti-symmetric stretch band at around 1160 cm^{-1} ⁵⁸⁻⁶⁰ but it is not recognized in the $|\chi^{(2)}|^2$ spectra measured. It is probably due to the weak

Raman activity of this vibration (Fig. S5). Therefore, we focus on the 1040 cm^{-1} band in the following discussion about the structure of the acetonitrile/platinum interface with $0.1\text{ M LiCF}_3\text{SO}_3$ electrolyte.

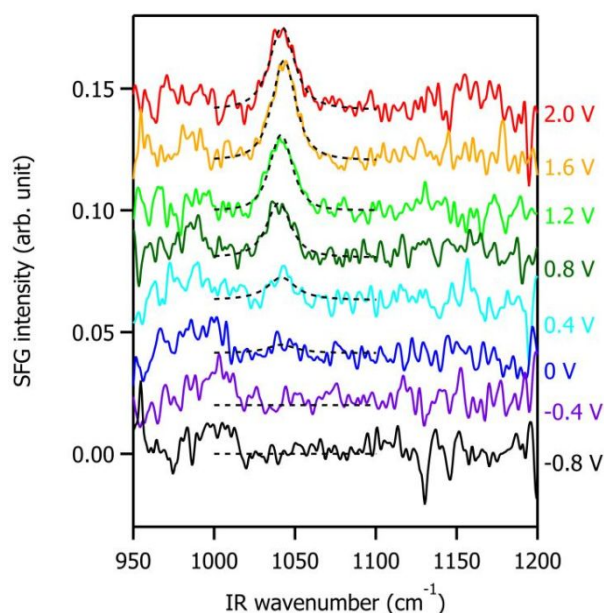


Fig. 7 VSFG intensity spectra of acetonitrile/platinum with $0.1\text{ M LiCF}_3\text{SO}_3$ in the anion band frequency region. The sample spectra are normalized by an air/gold spectrum. Black broken curves are fitted curve obtained by the square of Lorentz function. 0.02 offsets are added for the comparison of spectra. The potential is quoted against Ag/Ag^+ .

3-6. Structure of the acetonitrile/platinum interface

By gathering information obtained in the present study, we can now discuss the structure of the acetonitrile/platinum interface with $0.1\text{ M LiCF}_3\text{SO}_3$ electrolyte. Figure 8 compares the amplitudes of the CH_3 symmetric stretch, CN stretch (at 2245 cm^{-1}), CN^- stretch and SO_3^- symmetric stretch bands observed at different electrode potentials, which were obtained by the fitting analysis. (Details of the fitting analysis are described in SI.) As clearly seen, the amplitude of the CH_3 , SO_3^- , and CN bands increase as the electrode potential becomes more positive, in a manner similar to each other. This indicates that the amplitude of the vibrational bands of acetonitrile and the anion are strongly correlated. In contrast, the potential dependence of the broad negative CN^- band is clearly different from those of other bands, confirming that this band arises from a species different from free acetonitrile. Furthermore, the signal due to CN^- decreases in accordance with the increase of the signals due to the CF_3SO_3^- anion and acetonitrile, implying that the interface structure changes with the change of the potential applied to the platinum electrode.

Based on the above potential dependence of different interfacial species, we propose the structure at the acetonitrile/platinum interface with LiCF_3SO_3 electrolyte as illustrated in Fig. 9. At the negative potential, the interface does not have any distinct structure except that a small amount of

acetonitrile is decomposed to the CN^- anion on defect sites of the electrode and is adsorbed on the electrode.¹⁴ The acetonitrile molecules in the vicinity of the electrode exhibit no preferential orientation. On the other hand, at the positive potentials, the platinum electrode surface is covered by the CF_3SO_3^- anions, repelling the CN^- anion. The adsorbed CF_3SO_3^- anions interact with acetonitrile molecules and make them oriented with their CH_3 group pointing toward the anions on the electrode. Consequently, acetonitrile has net CH_3 -down and CN -up orientation in the vicinity of the platinum electrode. It is not clear why the acetonitrile does not show any net orientation at the interface at the negative potentials at the moment. One possibility is that because the charge of the electrode surface is well-delocalized and uniformly distributed, the charge density may not be high enough to induce a particular orientation of acetonitrile with a detectable magnitude. It might also be possible that the solvated cation in the vicinity of the electrode disturbs solvent orientation at the negative potentials.

Lastly, we mention the importance of complementary theoretical study to obtain a complete molecular-level picture of the electrolyte/electrode interface. For the air/water interfaces, in fact, it has been shown that combination of HD-VSFG spectroscopy and MD-simulation is indispensable for elucidating the interface structure.^{61, 62} For the acetonitrile/platinum interface investigated in this study, for example, the orientation of CN^- cannot be determined only from the experimental $\text{Im}\chi^{(2)}$ because the hyperpolarizability of cyanide is not known. DFT calculation of the system including the transition metal electrode is required for obtaining reliable hyperpolarizability of CN^- for discussing the orientation of the adsorbed CN^- .

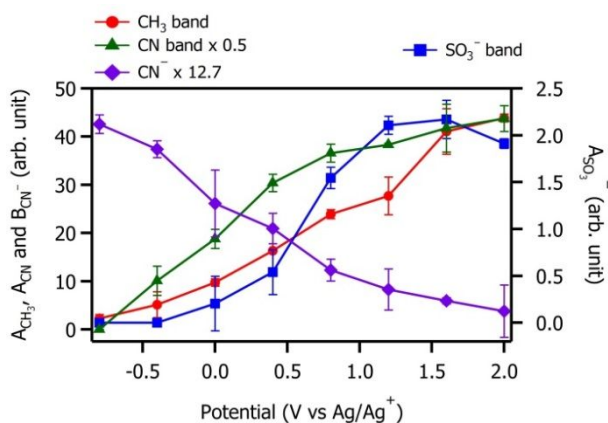


Fig. 8 Electrode potential dependence of the amplitudes of the CH_3 stretch (red circle), the CN stretch (green triangle) bands of free acetonitrile, the CN^- (purple diamond) and SO_3^- (blue square) bands in the spectra of acetonitrile/platinum interface with 0.1 M LiCF_3SO_3 electrolyte. The data points are averages of two negative-going scans from 2.0 V to -0.8V. The error bars indicate the variations between the two experiments at each potential.

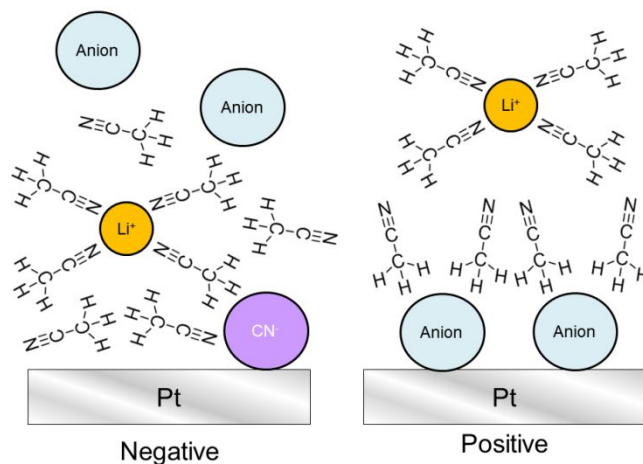


Fig. 9 Schematics of the structure of the acetonitrile/platinum interface with LiCF_3SO_3 electrolyte.

Conclusions

We realized HD-VSFG measurements at an electrolyte/electrode interface by employing the in-situ reference method, and succeeded in the observation of the potential-dependent orientation of the interfacial molecule for the first time. Electrochemical HD-VSFG measurements at the acetonitrile/platinum interface with 0.1 M LiCF_3SO_3 electrolyte revealed that the acetonitrile is pointing their CH_3 group toward the positively charged electrode. Because the signal intensity due to this oriented acetonitrile is well correlated with that of the CF_3SO_3^- anion adsorbed at the interface, we propose that this CH_3 -down orientation of the interfacial acetonitrile is induced by the anion adsorption on the electrode surface. The present study suggests that the essential role of the anion adsorption for determining the property of solvent molecules at the electrode interface. This work demonstrates that HD-VSFG spectroscopy is a very powerful method also for elucidating the structure at electrolyte/electrode interfaces at the molecular level.

Conflicts of interest

There are no conflicts to declare.

Acknowledgements

This work was supported by JST ALCA-SPRING and JSPS KAKENHI Grant No. 18H05265. RIKEN advanced manufacturing support team is acknowledged for making our spectro-electrochemical cell. RIKEN emergent matter science research support team is acknowledged for the use of electron beam evaporator for preparation of the sample electrode. This work was supported by RIKEN Junior Research Associate Program. SN acknowledges Prof. S. Baldelli for the valuable discussions.

References

1. Y. Yamada, J. Wang, S. Ko, E. Watanabe and A. Yamada, *Nature Energy*, 2019, **4**, 269.
2. Y. Zhang, M. Konya, A. Kutsumura, S. Lim, T. Mandai, H. Munakata and L. Kanamura, *small*, 2019, **15**, 1902236.
3. K. R. Adair, C. Zhao, M. N. Banis, Y. Zhao, R. Li, M. Cai and X. Sun, *Angew. Chem. Int. Ed.*, 2019, **58**, 1-7.
4. T. Kondo, T. Masuda, N. Aoki and K. Uosaki, *J. Phys. Chem. C*, 2016, **120**, 16118-16131.
5. S. Florencio, A. Jose, V. Maria, C. G. R., U. Antonio, F. Romero and A. J., *Electrochim. Acta*, 2018, **281**, 133-141.
6. P. J. C., A. Robert, D. W. M., D. S. W., B. H. E. A. and S. Neeraj, *J. Mater. Res.*, 2015, **30**, 381-389.
7. Y. X. Chen, A. Miki, S. Ye, H. Sakai and M. Osawa, *J. Am. Chem. Soc.*, 2003, **125**, 3680-3681.
8. E. Boscheto, B. C. Batsista, R. B. Lima and H. Varela, *J. Electroanal. Chem.*, 2010, **642**, 17-21.
9. S. J. Huo, X. K. Xue, Y. G. Yan, Q. X. Li, M. Ma, W. B. Cai, Q. J. Xu and M. Osawa, *J. Phys. Chem. B*, 2006, **110**, 4162-4169.
10. K. Nakata, Y. Kayama, K. Shimazu, A. Yamakata, S. Ye and M. Osawa, *Langmuir*, 2008, **24**, 4358-4363.
11. K. N. Heck, B. G. Janesko, G. E. Scuseria, N. J. Halas and M. S. Wong, *J. Am. Chem. Soc.*, 2008, **130**, 16592-16600.
12. X. Li, D. Heryadi and A. A. Gewirth, *Langmuir*, 2005, **21**, 9251-9259.
13. R. Gomez, J. S. Gullon, J. M. Perez and A. Aldaz, *ChemPhysChem*, 2005, **6**, 2017-2021.
14. R. A. Gu, P. G. Cao, Y. H. Sun and Z. Q. Tian, *J. Electroanal. Chem.*, 2002, **528**, 121.
15. Y. R. Shen, *The principles of Nonlinear Optics*, John Wiley & Sons, Inc: New York, 1984.
16. X. D. Zhu, H. Suhr and Y. R. Shen, *Phys. Rev. B*, 1987, 3047-3050.
17. J. H. Hunt, P. G. Sionnest and Y. R. Shen, *Chem. Phys. Lett.*, 1987, **133**, 189-192.
18. Y. R. Shen and V. Ostroverkhov, *Chem. Rev.*, 2006, **106**, 1140-1154.
19. A. A. Liu, S. Liu, R. Zhang and Z. Ren, *J. Phys. Chem. C*, 2015, **119**, 23486-23494.
20. J. Schaefer, G. Gonella, M. Bonn and E. H. G. Backus, *Phys. Chem. Chem. Phys.*, 2017, **19**, 16875-16880.
21. G. Neri, P. M. Donaldson and A. J. Cowan, *J. Am. Chem. Soc.*, 2017, **139**, 13791-13797.
22. C. S. Tian and Y. R. Shen, *Chem. Phys. Lett.*, 2009, **470**, 1-6.
23. M. Sovago, E. Vartiainen and M. Bonn, *J. Chem. Phys.*, 2010, **133**, 229901.
24. S. Nihonyanagi, S. Yamaguchi and T. Tahara, *J. Chem. Phys.*, 2009, **130**, 204704.
25. S. Nihonyanagi, S. Yamaguchi and T. Tahara, *Chem. Rev.*, 2017, **117**, 10665-10693.
26. A. Myalitsin, S. Urashima, S. Nihonyanagi, S. Yamaguchi and T. Tahara, *J. Phys. Chem. C*, 2016, **120**, 9357-9363.
27. S. Urashima, A. Myalitsin, S. Nihonyanagi and T. Tahara, *J. Phys. Chem. Lett.*, 2018, **9**, 4109-4114.
28. Y. Nojima, Y. Suzuki, M. Takahashi and S. Yamaguchi, *J. Phys. Chem. Lett.*, 2017, **8**, 5031-5034.
29. M. Okuno and T. Ishibashi, *J. Phys. Chem. C*, 2015, **119**, 9947-9954.
30. I. V. Stiopkin, C. Weeraman, P. A. Pieniazek, F. Y. Shalhout, J. L. Skinner and A. V. Benderskii, *Nature*, 2011, **474**, 192-195.
31. L. Götte, K. M. Parry, W. Hua, D. Verreault, H. C. Allen and D. J. Tobias, *J. Phys. Chem. A*, 2017, **121**, 6450-6459.
32. F. Dederichs, K. A. Friedrich and W. Daum, *J. Phys. Chem. B*, 2000, **104**, 6626-6632.
33. S. Baldelli, G. Mailhot, P. Ross, Y. R. Shen and G. A. Somorjai, *J. Phys. Chem. B*, 2001, **105**, 654-662.
34. S. Baldelli, G. Mailhot, P. N. Ross and G. A. Somorjai, *J. Am. Chem. Soc.*, 2001, **123**, 7697-7702.
35. S. Nihonyanagi, S. Ye, K. Uosaki, L. Dreesen, C. Humbert, P. Thiry and A. Peremans, *Surf. Sci.*, 2004, **573**, 11-16.
36. Z. D. Schultz, S. K. Shaw and A. A. Gewirth, *J. Am. Chem. Soc.*, 2005, **127**, 15916-15922.
37. H. Noguchi, T. Okada and K. Uosaki, *Faraday Discuss.*, 2008, **140**, 125-137.
38. F. Vidal, A. Tadjeddine, C. Humbert, L. Dreesen, A. Peremans, P. A. Thiry and B. Busson, *J. Electroanal. Chem.*, 2012, **672**, 1-6.
39. B. G. Nicolau, N. García-Rey, B. Dryzhakov and D. D. Dlott, *J. Phys. Chem. C*, 2015, **119**, 10227-10233.
40. T. Iwahashi, Y. Miwa, W. Zhou, Y. Sakai, M. Tamagata, M. Ishikawa, D. Kim and Y. Ouchi, *Electrochem. Commun.*, 2016, **72**, 54-58.
41. Y. Horowitz, H. Han, P. N. Ross and G. A. Somorjai, *J. Am. Chem. Soc.*, 2016, **138**, 726-729.
42. S. A. Sorenson, J. G. Patrow and J. M. Dawlaty, *J. Am. Chem. Soc.*, 2017, **139**, 2369-2378.
43. W. Xiong, J. E. Laaser, R. D. Mehlenbacher and M. T. Zanni, *PNAS*, 2011, **108**, 20902.
44. S. Nihonyanagi, A. Sayama, Y. Ohshima and T. Tahara, *Chem. Lett.*, 2019, **48**, 1387-1390.
45. P. Venkateswarlu, *J. Chem. Phys.*, 1951, **19**.
46. R. Raval and M. A. Chesters, *Surf. Sci.*, 1989, **219**, L505-L514.
47. K. Saito, Q. Peng, L. Qiao, L. Wang, T. Joutsuka, T. Ishiyama, S. Ye and A. Morita, *Phys. Chem. Chem. Phys.*, 2017, **19**, 8941-8961.
48. Y. R. Shen, *Fundamentals of Sum-Frequency Spectroscopy*, Cambridge University Press, 2016.
49. S. Yamaguchi, K. Shiratori, A. Morita and T. Tahara, *J. Chem. Phys.*, 2011, **134**, 184705.
50. K. Matsuzaki, S. Nihonyanagi, S. Yamaguchi, T. Nagata and T. Tahara, *J. Chem. Phys.*, 2019, **151**, 064701.
51. A. Tadjeddine, A. Le Rille, O. Pluchery, F. Vidal, W. Q. Zheng and A. Peremans, *Phys. Stat. Sol. (a)*, 1999, **175**, 89.
52. H. J. Herrera-Suarez, A. Rubio-Ponce and D. Olguin, *Rev. Mex. Fis.*, 2012, **58**, 46-54.
53. A. T. Hubbard, E. Y. Cao and D. A. Stern, *Electrochim. Acta*, 1994, **39**, 1007-1014.
54. N. M. Markovic, H. A. Gasteiger and P. N. Ross, *J. Phys. Chem.*, 1996, **100**, 6715-6721.
55. B. Bozzini, B. Busson, A. Gayral, C. Humbert, C. Mele, C. Six and A. Tadjeddine, *Molecules*, 2012, **17**, 7722-7736.
56. F. Dederichs, A. Petukhova and W. Daum, *J. Phys. Chem. B*, 2001, **105**, 5210-5216.
57. E. C. Ou, P. A. Young and P. R. Norton, *Surf. Sci.*, 1992, **277**, 123-131.
58. D. H. Johnston and D. F. Shriver, *Inorg. Chem.*, 1993, **32**, 1045-1047.
59. J. M. Alia, Y. D. Mera, H. G. M. Edwards, F. J. Garcia and E. E. Lawson, *J. Mol. Struct.*, 1997, **408/409**, 439-450.

ARTICLE

Journal Name

60. P. Geetha, M. Nair, C. Y. Panicker, H. T. Varghese, S. M. Y., K. Raju and P. S. A. Devi, *Orient. J. Chem.*, 2010, **26**, 167-170.
61. K. Inoue, T. Ishiyama, S. Nihonyanagi, S. Yamaguchi, A. Morita and T. Tahara, *J. Phys. Chem. Lett.*, 2016, **7**, 1811-1815.
62. R. Kusaka, T. Ishiyama, S. Nihonyanagi, A. Morita and T. Tahara, *Phys. Chem. Chem. Phys.*, 2018, **20**, 3002-3009.